Bone 83 (2016) 82–92

Contents lists available at ScienceDirect

Bone

journal homepage: www.elsevier.com/locate/bone

Original Full Length Article

Monitoring immune responses in a mouse model of fracture fixation with and without *Staphylococcus aureus* osteomyelitis☆

Edward T.J. Rochford [a], Marina Sabaté Brescó [a,b], Stephan Zeiter [a], Katharina Kluge [a], Alexandra Poulsson [a], Mario Ziegler [b], R. Geoff Richards [a], Liam O'Mahony [b,1], T. Fintan Moriarty [a,*,1]

[a] AO Research Institute Davos, Switzerland
[b] Swiss Institute of Allergy and Asthma Research (SIAF), University of Zurich, Davos, Switzerland

ARTICLE INFO

Article history:
Received 7 June 2015
Revised 21 September 2015
Accepted 11 October 2015
Available online 23 October 2015

Keywords:
Host responses
Pathogenesis
S. aureus
Fracture
Trauma
Osteosynthesis
Biofilm
Osteomyelitis
Implant associated infections

ABSTRACT

Post-traumatic bone fractures are commonly fixed with implanted devices to restore the anatomical position of bone fragments and aid in the healing process. Bacterial infection in this situation is a challenge for clinicians due to the need for aggressive antibiotic therapy, debridement of infected tissues, and the need to maintain fracture stability. The aim of this study was to monitor immune responses that occur during healing and during *Staphylococcus aureus* infection, in a clinically relevant murine model of fracture fixation.

Skeletally mature C57bl/6 mice received a transverse osteotomy of the femur, which was treated with commercially available titanium fracture fixation plates and screws. In the absence of infection, healing of the fracture was complete within 35 days and was characterized by elevated Interleukin (IL)-4 and Interferon-gamma secretion from bone-derived cells and expression of these same genes. In contrast, mice inoculated with *S. aureus* could not heal the fracture within the observation period and were found to develop typical signs of implant-associated bone infection, including biofilm formation on the implant and osteolysis of surrounding bone. The immune response to infection was characterized by a T_H17-led bone response, and a pro-inflammatory cytokine-led Tumor necrosis factor (TNF)-α, Interleukin (IL)-1β) soft tissue response, both of which were ineffectual in clearing implant related bone and soft tissue infections respectively.

In this murine model, we characterize the kinetics of pro-inflammatory responses to infection, secondary to bone trauma and surgery. A divergent local immune polarization is evident in the infected versus non-infected animals, with the immune response ultimately unable to clear the *S. aureus* infection.

1. Introduction

Infection is a major cause of medical device failure. In orthopedic medicine, 1–5% of all patients receiving devices develop an infection [1]. The highest infection rates are observed in severe open fractures fixed with devices such as fracture fixation plates [2]. In the majority of cases, infections related to orthopedic devices are caused by common members of the normal human skin microflora, e.g. *Staphylococcus aureus*, and it is known that the presence of an implanted device significantly lowers the number of these opportunistic pathogens required to cause infection [3].

Experimental studies have revealed a number of factors that likely play important roles in the progression of implant associated bone infections. These include bacterial biofilms that are recalcitrant to host defenses and antimicrobial drugs [4], and which have also been shown to skew monocytes/macrophages toward alternatively activated M2 phenotype [5]. More recently, it has also been shown in experimental studies that myeloid-derived suppressor cells (MDSCs) function in an immunosuppressive manner in implant related *S. aureus* bone infection and this limits monocyte/macrophage pro-inflammatory activity [6]. Finally, pro-inflammatory T_H1/T_H17 and down regulated T_H2 and regulatory T cell responses (Treg) responses appear to play a role in the development of chronic implant-related bone infection in mice [7].

In the particular case of infection after surgically fixed bone fractures however, it is important to note that the trauma leading to the fracture [8,9]; the stress of surgically placing the device [10]; the biomechanical stability of the resultant implant construct and the downstream effects on bone healing [11], all have an impact on the immune status and response of the host. In particular, fracture healing progresses through an early inflammatory phase characterized by peripheral mononuclear (PMN) cell recruitment and pro-inflammatory cytokine secretion (mainly tumor necrosis factor (TNF)-α, interleukin (IL)-1β, IL-6) [12]. Healing then proceeds to a more anti-inflammatory phase characterized by the secretion of anti-inflammatory cytokines such as IL-10 and

☆ Conflicts of interest: none.

* Corresponding author at: AO Research Institute Davos, AO Foundation, Clavadelerstrasse 8, Davos Platz, CH7270, Switzerland.
E-mail address: fintan.moriarty@aofoundation.org (T.F. Moriarty).

[1] Contributed equally.

http://dx.doi.org/10.1016/j.bone.2015.10.014
8756-3282/

transforming growth factor (TGF)-β, angiogenic factors e.g. platelet-derived growth factor (PDGF) and recruitment of macrophages and other cell types [13]. Considering the dual role played by many of these cells and cytokines, it is therefore likely that the above-mentioned factors (trauma, bone damage, healing and biomechanics) may also play a role in the risk and progression of infection. Numerous animal models have been used to investigate both acute [14] and chronic [15] device related osteomyelitis [16–19], however, in many such models, the "device" used is a simple wire, or pin, and is placed through the bone with a co-administered bacterial inoculum. In most cases therefore, there is no fracture, and the implant functions merely as a foreign body, rather than as a clinically relevant fracture fixation device.

In order to further our understanding of infection development and host responses after fracture fixation, experimental models that incorporate these factors under controlled conditions are required. The aim of this study was to characterize a murine model of infection after fracture fixation that includes bone damage (osteotomy), biomechanical loading and a clinically realistic fixation device [20,21]. The model was used to provide a more complete understanding of the progression of fracture healing under clinically relevant conditions and how healing and immune responses are affected in the presence of *S. aureus* contamination and subsequent infection.

2. Experimental procedures

2.1. Animal care and use

Consent to perform this study was granted by the ethical committee of the canton of Grisons in Switzerland and was carried out in an AAALAC accredited research institute. Skeletally mature, female, specific pathogen free (SPF) C57bl/6 mice (20–28 weeks old), purchased from Charles River (Germany) were used in this study. All animals were allowed to acclimatize to experimental conditions for two weeks prior to the start of the study. Mice were housed under a 12 h dark/12 h light cycle in groups of six in individually ventilated cages and re-housed in the same groups post-surgery. Animals were fed with a standard diet (Provimi, Switzerland) and had free access to water at all times. Six mice were analyzed per time-point (1, 3, 7, 14, 21, 28 and 35 days) and for each time-point there were 2 groups: infected and non-infected. Implants were placed on the left femur (unilateral model, described below). In addition to the animals receiving implants, a group of six healthy, non-operated animals were used to establish baseline values for the RT-qPCR, cytokine and lymphocyte measurements.

2.2. Implants

Commercially pure Titanium (CpTi) 4-hole rigid Mousefix plates and Titanium Aluminum Niobium alloy (Ti6Al4Nb (TAN)) screws were used in this study (RISystem AG, Switzerland). Prior to placement, the plates and screws were cleaned by sonication (2 × 15 min each) in a series of propan-2-ol, 70% (*v*/*v*) ethanol and ultrapure water. The materials and surgical equipment were sterilized by steam autoclave before use.

2.3. Bacterial inoculation

A clinical *S. aureus* isolate, JAR06.01.31, which was originally cultured from an infected hip prosthesis, was selected as the test organism [22,23]. The bacterial inoculum was introduced to the mice on pre-contaminated Mousefix plates using the following method. A single colony of *S. aureus* JAR06.01.31 was grown for 18 h at 37 °C, 100 rpm in tryptic soy broth (Sigma Aldrich, Switzerland). The resulting bacterial suspension was then washed by centrifugation 3 times (2500 *g*), each time re-suspended in phosphate buffered saline (0.5 M PBS, pH 7.4), as previously described [24]. The suspension was then adjusted to an optical density of 1.15 (±0.03) at 600 nm using a spectrophotometer (Multiskan Go, Thermo Scientific, Switzerland), equivalent to approximately 4×10^8 colony forming units (CFU) per mL. The plates were completely submerged in the bacterial suspension and incubated statically at room temperature for 20 min. The implants were subsequently air dried under sterile conditions in a laminar flow hood for 5 min. This procedure was confirmed to reproducibly yield 9×10^5 (± standard deviation 2.6×10^5) CFU per implant. For surgery, the implants were mounted in drill and saw guide jigs (RISystem AG, Switzerland) with a piece of polyglactin 3–0 suture material (Ethicon, Switzerland). All of the implants were placed within 4 h of bacterial contamination. The time differential did not affect bacterial viability (data not shown).

2.4. Surgery and post-operative care

Surgery was performed under inhalation anesthesia, which was induced by placing mice in a plexiglass induction box flooded with 3% isoflurane (Isofluran Baxter®, Baxter AG, Switzerland) in 100% O_2. Animals were placed on a heating pad and anesthesia was maintained with 1.5–2% isoflurane in 100% O_2 delivered via a rodent facemask at 0.5–0.8 L min^{-1}. In addition, buprenorphine (Temgesic®, Reckitt Benckiser AG, Switzerland, 0.1 mg kg^{-1}) was administered subcutaneously. The surgery was then conducted as described [20] and in accordance with manufacturer protocols (RISystem AG, Switzerland, available online at risystem.com). Briefly, the animal was placed in prone position. A skin incision was made from tail base to left stifle. The subcutaneous Fascia lata was cut and the tissue plane between the quadriceps and the biceps femoris muscle was bluntly dissected. This gave access to the lateral aspect of the femur. A Teflon foil was placed under the femur to protect the soft tissue from contamination. The plate was then fixed to the bone using four self-tapping, angular stable screws. Screw holes were predrilled with a 0.31 mm drill bit. No irrigation was applied during drilling or sawing in order to prevent the spread of bacteria into the surrounding soft tissue. Once the plate was in place, a 0.44 mm defect osteotomy was performed using a jig and a Gigly wire. The foil was then removed and the Fascia lata and the skin were closed with continuous sutures (5–0 Vicryl rapide, Ethicon, Belgium). In the infected animals, a new set of sterile instruments were used for wound closure. Following surgery, a lateral radiograph of the femur was taken to confirm proper positioning of the implant and the fracture gap. Postoperative analgesia was provided in the form of subcutaneous buprenorphine (0.1 mg kg^{-1}) every 6–8 h for 16 h and a palatable form of acetaminophen (Dafalgan Syrup for Children, Bristol-Myers Squibb SA, Switzerland) (2 mg mL^{-1}) was added to the drinking water for 7 days. Animals recovered from anesthesia under close supervision, and their appearance, behavior, wound healing, food and water intake were monitored twice daily for a week, and subsequently once a day using a detailed numerical scoring system. Weights and radiographs of the operated limb were taken weekly.

2.5. Histology

Sixteen animals were operated to provide sections for histopathological evaluation of infected and control animals (n = 4 per group, per time-point). Animals were sacrificed at 3 and 7 days to evaluate the acute phase of the infection. Immediately after euthanasia, the entire operated femur and surrounding musculature underwent immediate fixation with 70% (*v*/*v*) methanol. Contact radiographs were taken of the entire specimen using high resolution technical films (D4 Structurix DW ETE, Agfa, Belgium) and a cabinet X-ray system (Model No. 43855A, Faxitron X-Ray Corporation, USA). Following fixation, samples were dehydrated through an ascending series of ethanol, transferred to xylene, and finally infiltrated with and embedded in polymethylmethacrylate (PMMA) [25]. The polymerized blocks were cut using an annular blade saw (Leitz 1600 saw microtome, Leica AG, Switzerland) resulting in 1 longitudinal cut through the plate per femur. Finally, each section was glued with cyanoacrylate

onto plexiglass slides, ground and polished down to approximately 100 μm using a micro-grinding system (Exact®, Germany) and stained with Giemsa/Eosin (GE).

2.6. Light microscopic analysis

Qualitative histopathological analysis was performed using a light microscope (Olympus, Switzerland). Histological findings were described, wherever possible, according to distribution, severity and morphologic character. The histopathological analysis included the hard and soft tissue, with special emphasis on character and localization of inflammatory changes and on bacterial colonization.

2.7. Sample harvesting and preparation

At each scheduled time-point, the animals were euthanized after inducing general anesthesia in an induction box (5% isoflurane in 100% O_2, 1 L min^{-1}) before cervical dislocation. A lateral radiograph of the left femur with implant in place was acquired post mortem. The following tissues were harvested: the operated femur with implant in place, the soft tissue surrounding the implant, the popliteal lymph node, and the spleen. The implant was then separated from the femur and placed in a sterile container. All tissue samples were immediately placed on ice in individual PBS-containing vials. The popliteal lymph nodes from the non-infected mice were pooled (according to treatment group and time-point) in order to obtain sufficient cell numbers for analysis as sufficient cell counts were not retrieved in the absence of infection. The tissue samples were subsequently mechanically homogenized (Omni Tissue Homogenizer and Hard Tissue Homogenizing tips, Omni International, USA) to give single cell suspensions.

2.8. Quantitative microbiology

The number of bacteria associated with the implant was determined by sonicating the plate and screws in PBS for 3 min (Bandelin Sonorex at 40 kHz) and vortex mixing for 20 s before performing serial dilution and viable plate counts on 5% horse blood agar (Oxoid, Switzerland). The quantity of bacteria associated with the soft tissue and femur was determined by taking a sample of the homogenized tissue, centrifuging at 2500 *g* for 10 min, re-suspending in 200 μL ultrapure water and incubating for 15 min at room temperature to lyse any eukaryotic cells that may harbor intracellular bacteria. Following this incubation, 200 μL of 1.8% NaCl was added and the bacteria were re-suspended and quantified by plating serial dilutions on blood agar plates.

All agar plates were incubated for 24 h at 37 °C and any subsequent bacterial growth checked for contamination or signs of co-infection. Identification of the bacteria growing in culture-positive samples was performed for at least one colony from each culture positive animal, by a *S. aureus* latex agglutination assay (Staphaurex, by Remel, Thermo Scientific, Switzerland).

2.9. Cell isolation

The homogenized femur, soft tissue, spleen and lymph nodes were ground through a 70 μm grid size cell strainer (BD, Switzerland) before being centrifuged at 270 *g* at room temperature. The pellet was subsequently re-suspended in 1 mL complete RPMI (cRPMI: RPMI 1640 (Sigma, Switzerland), penicillin (1 U mL^{-1}, Sigma, Switzerland), streptomycin (1 μg mL^{-1}, Sigma, Switzerland), kanamycin (0.1 μg mL^{-1}, Gibco, Switzerland), MEM vitamin, L-glutamine (2 mM, Sigma, Switzerland), Na-pyruvate (1 mM, Sigma, Switzerland), non-essential amino acids and heat inactivated fetal calf serum (10%, Sigma, Switzerland). The cell density was assessed using a Sysmex KX1 cell counter and adjusted with cRPMI to the following values mL^{-1}: femur, 1.5×10^6; soft tissue, 2×10^6; spleen, 1×10^6, lymph nodes, 1×10^6.

2.10. Flow cytometry analysis

The lymph node and spleen derived single cell suspensions were stimulated with 50 ng mL^{-1} PMA, 500 ng mL^{-1} ionomycin in the presence of 0.5 μL brefeldin A (to prevent the cells from secreting cytokines) (Biolegend, Switzerland) for 4 h at 37 °C, 5% CO_2. The cell suspensions were washed with 0.5 mL of 1% fetal calf serum and centrifuged at 300 *g* for 5 min. Cells were stained according to manufacturer's instructions with antibodies for CD3 (PeCy7 anti-mouse CD3ε, Biolegend, CH) and CD4 (Pacific blue anti-mouse CD4, Biolegend, Switzerland). Following fixation with intracellular fixation buffer (Biolegend, CH) and permeabilization of the cells with Permeabilization buffer (Biolegend, CH), the lymph node cells were stained for IL-4 (anti-mouse IL-4 APC, eBiosciences, Switzerland), IL-10 (anti-mouse IL-10 PE, eBiosciences, CH), IL-17A (anti-mouse IL-17A Alexa Fluor 488, eBiosciences, Switzerland) and IFN-γ (anti-mouse IFN-γ PerCP-Cy5.5, eBiosciences, CH), according to manufacturer protocols. The cells were washed and re-suspended in MACS buffer (Mitenyi Coulter, Switzerland) and a Gallios flow cytometer (Beckman Coulter, Switzerland) was used to measure cellular fluorescence with data processing by Kaluza software (Beckman Coulter, Switzerland). The results were expressed as percentage of the total cell number.

2.11. RT-qPCR

Femur and soft tissue samples were prepared by centrifuging 330 μL of cell suspensions at 730 *g* for 3 min. The supernatant was replaced and cells lysed with 350 μL of RLT buffer (Qiagen, Switzerland) supplemented with 0.01% β-mercaptoethanol (Roth, Germany). Total RNA was isolated from cell lysates using Qiagen RNeasy plus mini kits (Qiagen, Switzerland) followed by reverse transcription reaction performed in Eppendorf Mastercycler Gradient (Vaudaux-Eppendorf, Switzerland). RT-PCR was performed using SYBR green and a 7900HTFast Real-Time PCR system (Applied Biosciences, Switzerland). The following cytokine primers were used: Glyceraldehyde 3-phosphate dehydrogenase (GAPDH), IL-1β, IL-4, IL-10, IL-12p35, IL-12p40, IL-17A, interferon (IFN)-γ and TNF-α (Table 1). Equivalent data was also generated for platelet-derived growth factor B (PDGF-B) and transforming growth factor beta 1(TGF-β 1) (Table 1, Supplementary Fig. 1). The data was processed using SDS software (Applied Biosystems, Switzerland) results presented as 2-ΔΔCt values normalized to the expression of GAPDH and negative control samples. GAPDH was used as it was found not to vary throughout the samples in these experiments.

Table 1
The primers used in this in vivo study for RT-PCR analysis using SYBR green.

Primer	Template (5′-3′)	Company
GAPDH fw	TGC ACC ACC AAC TGC TTA G	Microsynth AG, CH
GAPDH rv	GGA TGC AGG GAT GAT GTT C	Microsynth AG, CH
IL-1β fw	AAG GAG AAC CAA GCA ACG ACA AAA	Microsynth AG, CH
IL-1β rv	TGG GGA ACT CTG CAG ACT CAA ACT	Microsynth AG, CH
IL-4 fw	GGC ATT TTG AAC GAG GTC ACA	Microsynth AG, CH
IL-4 rv	AGG ACG TTT GGC ACA TCC A	Microsynth AG, CH
IL-12p35 fw	GCT TCT CCC ACA GGA TT	Microsynth AG, CH
IL-12p35 rv	CTA GAC AAG GGC ATG CTG GT	Microsynth AG, CH
IL-17A fw	GTG TCA ATG CGG AGG GAA	Microsynth AG, CH
IL-17A rv	TTC AGG ACC AGG ATC TCT TGC T	Microsynth AG, CH
IFN-γ fw	CCC ACA GGT CCA GCG CCA AG	Microsynth AG, CH
IFN-γ rv	CAG CAG CGA CTC CTT TTC CGC T	Microsynth AG, CH
PDGF-B fw	CATCCGCTCCTTTGATGATCTT	Microsynth AG, CH
PDGF-B rv	GTGCTCGGGTCATGTTCAAGT	Microsynth AG, CH
TGF-beta 1 fw	CTCCCGTGGCTTCTAGTGC	Microsynth AG, CH
TGF-beta 1 rv	GCCTTAGTTTGGACAGGATCTG	Microsynth AG, CH
TNF-α	QuantiTect primer assay	Qiagen, CH

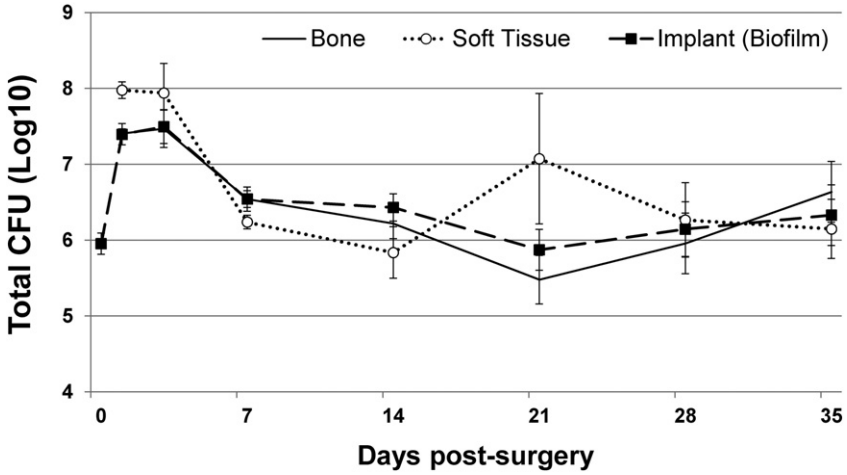

Fig. 1. Quantitative bacteriological culture results reveal persistence of infection in all locations. Mice received fracture fixation plates pre-colonized with 9×10^5 CFU *S. aureus* and at each scheduled euthanasia time point, the soft tissues, implants (plate and screws) and the bone were separated and processed individually for quantitative bacteriology ($n \geq 6$ at each time-point, mean ± s.d.).

2.12. Cell stimulation and cytokine secretion

An additional 330 μL aliquot of the femur and soft tissue single cell suspensions was taken and cells stimulated with 50 ng mL^{-1} phorbol 12-myristate 13-acetate (PMA, Sigma, Switzerland) and 500 ng mL^{-1} ionomycin (Sigma, Switzerland). Following incubation for 24 h at 37 °C, 5% CO_2, 50 μL of the cell culture supernatants were analyzed using a customized Bioplex kit for the following cytokines: IL-1β, IL-4, IL-6, IL-10, IL-12p70, IL-17A, IFN-γ and keratinocyte chemoattractant (KC), (BIORAD, Switzerland). Analysis was performed using a BIO-PLEX 200 system connected to a BIO-PLEX with high-throughput fluidics (BIORAD, Switzerland).

2.13. Statistical analysis

Results are presented as means of each group with standard deviations (s.d.). A two way ANOVA was used to compare differences between infected and non-infected groups versus un-operated controls for gene expression and cytokine secretion and Sidak's post-hoc test was used to control for multiple comparisons. For flow cytometry data, where cells from non-infected animals were pooled to yield sufficient numbers, change in cell number over time was measured by one way ANOVA. In all cases, significance was set at: *$P < 0.05$;***$P < 0.01$; ***$P < 0.001$, ****$P < 0.0001$. Prism software was used for all statistical tests (GraphPad Software Inc.; La Jolla, CA).

3. Results

3.1. Quantitative microbiology

All animals receiving a contaminated plate were found to be culture positive for *S. aureus* at the scheduled euthanasia time-points. No other bacterial species were identified in any animal. The number of bacteria cultured from the implant, femur and soft tissue was assessed and the results demonstrated that the quantity of bacteria present on the implant rapidly increased from the pre-implantation value (9×10^5 CFU/Implant) to approximately 2×10^7 CFU/Implant at 24 h (Fig. 1). Bacterial loads tended to peak between days 1 and 3 in all of the locations studied, with highest bacterial load in the soft tissue at these time-points. After the peak at day 3, bacterial numbers tended to decline 10 to 100 fold by day 21, after which the bacterial numbers appeared to plateau or even slightly increase again. A second peak was apparent in the soft tissues at day 21, but not at the other locations.

3.2. Radiographic and histological assessment of healing

Osteotomy healing, observed as bridging of the osteotomy gap, occurred between 14 and 21 days in non-infected animals, with complete healing observed at euthanasia on day 35 (Fig. 2). The infected animals on the other hand, displayed significant osteolysis and the osteotomy gap was clearly not healed as shown in radiographs at day 35 (Fig. 2).

Fig. 2. Healing of the osteotomy gap in non-infected mice versus osteolysis and failure to heal in infected mice. Radiographs of inoculated and non-infected mice were taken immediately post operatively (left) and after 35 days. The non-infected group (center) achieved osteotomy gap closure and complete healing by day 35, whilst infected animals (right) displayed a complete lack of osteotomy healing and significant bone damage at 35 days (D).

Histological sections also revealed significant differences between the infected and non-infected groups at early time-points (day 3 and day 7) and representative images are shown in Fig. 3. Non-infected mice displayed minimal inflammatory cell infiltration into the osteotomy site at day 3 (Fig. 3B), although an early fibrin network was observed. This fibrin network transitioned to a fibrous granulation tissue (Fig. 3H) in the osteotomy gap of non-infected mice by day 7, indicative of early stages of normal osteotomy healing, although no cartilage formation was observed at this time. In the infected group, the histological sections revealed that the osteotomy site displayed a moderate degree of inflammatory cell infiltration already by day 3 (Fig. 3 E), and by day 7 osteolysis and a high degree of inflammatory cell infiltration was observed (Fig. 3K). Concerning the soft tissues above the plate, a low grade, mixed cell (PMN and mononuclear) inflammation and minor acute myocytic degeneration (Zenker degeneration) was observed at day 3 in non-infected mice (Fig. 3C, white square). These features are indicative of a minor tissue insult as caused by the surgical procedure and placement of implants. By day 7, the inflammation above the plate had transitioned to a highly vascularized (Fig. 3I, white square) granulation tissue in non-infected mice, with relatively fewer PMN cells than in the infected group. In comparison, infected animals displayed a marked increase in PMN cells in the soft tissue above the plate at day 3 (Fig. 3F). By day 7 in the infected group, the soft tissue displayed signs of massive myocytic necrosis (debris) and early signs of fibroblast proliferation surrounding the entire plate (Fig. 3L, white asterisk).

Bacterial micro-colonies were visible in the Giemsa-Eosin stained sections at both day 3 and 7 in the infected group (day 7 shown in Fig. 4). Bacteria were primarily located adjacent to small bone fragments in the medullary cavity created during osteotomy and screw placement (Fig. 4 A, inset) and in the soft tissues above the plate (Fig. 4B). Thin biofilms of bacteria were also observed on the surface of the plate (Fig. 4B, inset).

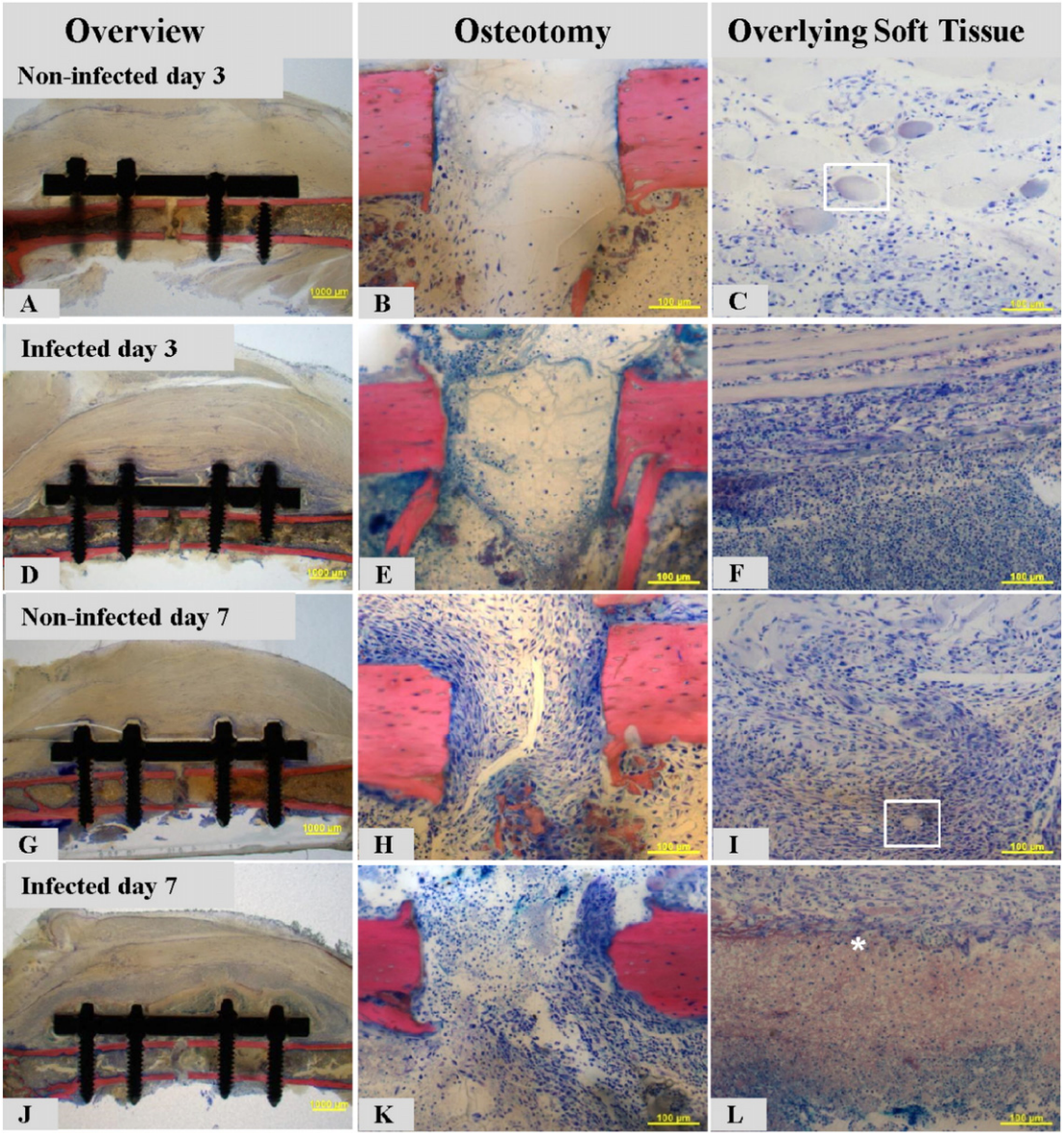

Fig. 3. Histological sections showing typical features of infected and non-infected mice at 3 and 7 days post-surgery. Overview images are shown on left (scale bar 1′000 μm) with the plate, four screws and central osteotomy visible. Higher magnification images of the osteotomy gap are shown in the center (scale bar 100 μm) and overlying soft tissue on right (scale bar 100 μm). See text for full description, highlighted items are: Zenker degeneration in non-infected mouse at day 3 indicative of normal post-surgical healing (white box in C); vascularization in overlying soft tissues in non-infected mouse at day 7 (white box in I) and interface between massive necrotic region and fibroblast proliferation in infected animals at day 7 (white asterisk in L). All samples were embedded in PMMA and sections were ground down to100μm and stained with Giemsa Eosin.

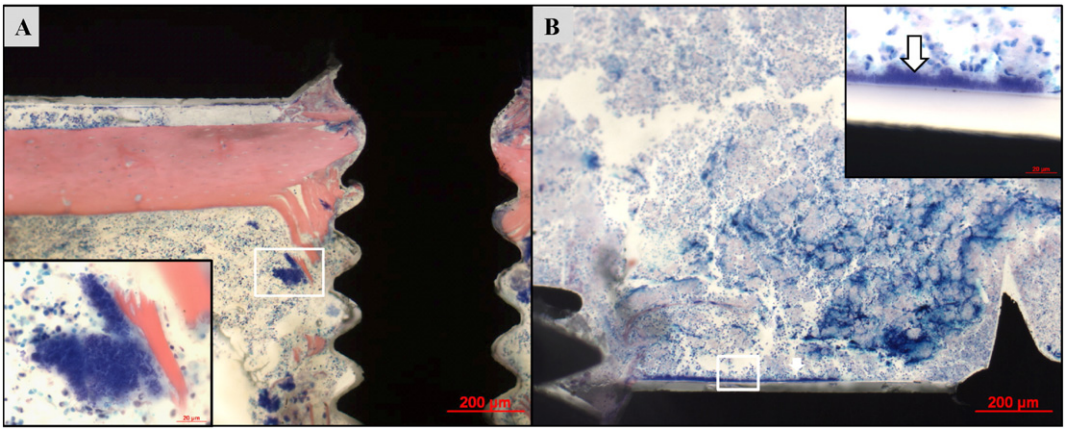

Fig. 4. Localization of bacteria in infected mice at day 7. A: bacteria tended to form micro-colonies surrounding small bone fragments created during screw placement (scale bar 200 μm, inset scale bar 20 μm). B: Large numbers of bacteria were observed in the necrotic tissue adjacent to the plate and as a biofilm directly above the plate (scale bar 200 μm, inset scale bar 20 μm). Deeply staining blue material is composed of bacterial micro-colonies and some nuclear material from necrotic cellular debris. Note shrinkage artifact visible between implant and biofilm. All samples were embedded in PMMA and sections were ground down to 100 μm and stained with Giemsa Eosin.

3.3. Adaptive immune responses within the lymph nodes

Total lymphocyte cell numbers in local lymph nodes and spleen were quantified in order to assess local and systemic immune activation respectively. In non-infected mice, the total number of lymphocytes isolated from lymph nodes and spleen remained similar at all time-points (Fig. 5A), indicating that the surgical procedure and implant placement did not induce a systemic response in the absence of infection. In contrast, the lymph node and spleen cell count in infected animals did not remain constant over time, but rather increased (Fig. 5A), reflective of a systemic response to the infection.

In order to better define the polarization of lymphocyte responses within the local lymph nodes, we performed intracellular cytokine staining on CD3 + CD4 + and CD3 + CD4 − lymphocytes. Other than an early (day 1 post surgery) temporary increase in IFN-γ and IL-4 positive lymphocytes, the local lymph nodes of non-infected mice displayed few fluctuations over time (Fig. 5B). In contrast, infected animals displayed significant fluctuations in lymphocyte subsets over time. IL17A positive and IL-10 positive lymphocytes were significantly increased at day 14, indicating the induction of an anti-bacterial T_H17 response and a regulatory lymphocyte subset (IL-10 positive lymphocytes). IL-4 and IFN-γ positive lymphocytes were significantly increased by day 28 in infected animals, suggesting an increase in T_H1 and T_H2 lymphocyte subsets respectively.

3.4. Cytokine gene expression

Gene expression analysis of selected cytokine genes in both bone and soft tissue samples revealed that non-infected mice displayed significant changes in IL-4 and IFN-γ expression, particularly within the soft tissue (Fig. 6). Infected animals on the other hand, displayed significant increases in expression of IL-17 in infected bone at later time-points, while both TNF-α and IL-1β gene expression were significantly increased in bone and even more so in soft tissues (Fig. 6). Gene expression data for IL-10, IL-12p35 and IL-12p40 were below detectable limits (data not shown). Indicators of bone healing, PDGF and TGF-β, were significantly increased during the healing phase in non-infected animals (7–21 days), whilst infected animals showed no change (TGF-β) or indeed a reduction (PDGF) in gene expression during this time (Supplementary Fig. 1).

Thus, the gene expression profile of non-infected mice was characterized by elevated IL-4 and IFN-γ expression, whilst infected mice appeared to be characterized by elevated IL-17, TNF-α and IL-1β.

3.5. Cytokine secretion

Cytokine secretion from ex vivo stimulated single cell suspensions from bone and soft tissue homogenates is shown in Fig. 7. *Ex vivo* cytokine secretion is useful in addition to tissue gene expression analysis, as ex vivo secretion indicates the magnitude and polarization of immune cell activation *in vivo*. In addition, cells that do not express specific cytokine genes *in vivo*, but can upregulate their cytokine gene expression and protein secretion when activated ex vivo, are assessed. Consistent with the gene expression data, *ex vivo* stimulated single cell suspensions from non-infected mouse bone secreted high levels of IL-4 immediately following surgery and high levels of secretion was observed at all time points thereafter. *Ex vivo* stimulated single cell suspensions from infected mouse bone also secreted high levels of IL-4 for 3 days following surgery, but the level of IL-4 secreted was reduced at day 7 and remained low for the remainder of the study. Interestingly, the drop in IL-4 secretion by infected bone single cell suspensions at day 7 was accompanied by a significant increase in IL-17 and IFN-γ secretion, suggesting a switch from a T_H2 dominant response to a mixed T_H17 and T_H1 response within infected bone at this time point. High levels of *ex vivo* stimulated IL-17 secretion was observed from infected bone for the remainder of the study, while IFN-γ secretion subsided from day 14. Secretion of the neutrophil chemotactic cytokine KC in infected mouse bone cells was elevated at day 35, but not in the non-infected samples. High levels of the anti-inflammatory cytokine IL-10 were also released from *ex vivo* stimulated infected mouse bone single cell suspensions, which was not observed for non-infected mouse bone cells.

Non-infected soft tissue samples did not release significant levels of any of the cytokines tested, however, IL-17 and KC secretion was significantly increased for *ex vivo* stimulated soft tissue cells from infected animals. This may possibly be due to the presence of inflammatory cells, which are not present in non-infected soft tissue (Fig. 3). IL-6 and IL-1β were also assayed but their levels were below the detection limit of the assay.

4. Discussion

Post-traumatic fractures of bone, and their subsequent repair with fixation devices (osteosynthesis), result in a host response that is a product of a number of contributing factors. These factors include the initial trauma and bone damage, the surgical intervention, device implantation (foreign body) and the biomechanics of the resultant implant construct. This complex interplay has a significant overarching immunological component, both during normal healing and during infection.

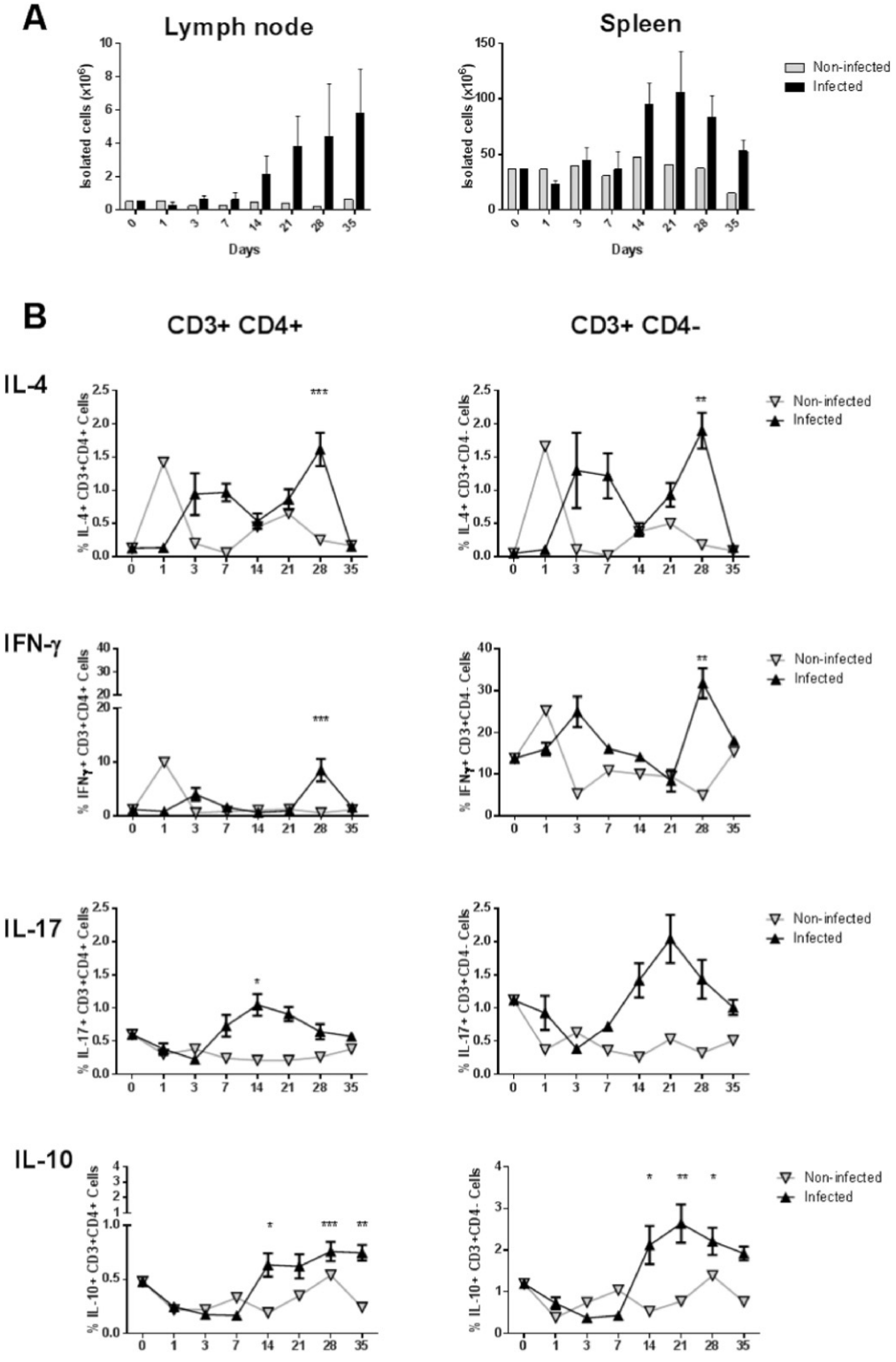

Fig. 5. A: Number of cells isolated from the popliteal lymph nodes (left) and spleens (right) of the infected and non-infected animal. B: Relative abundance of IL-4+, IFN-γ+, IL-17A+ and IL-10+ cells isolated from the popliteal lymph nodes was measured at each scheduled time-point after cell isolation, fixation and staining for intracellular cytokines. In the infected animals n = 6 ± s.d., in the non-infected animals the lymph nodes provided few cells and so all 6 samples were pooled. *; **P < 0.05; ***P < 0.01; ****P < 0.001: infected series versus infected day 1).

In this study, our aim was to establish a murine model of osteosynthesis, and investigate the key features of the immune response during healing and *S. aureus* infection.

The murine model used in this investigation has previously been shown to result in healing of the osteotomy within 14 to 21 days [26]. In this study, we show that healing proceeded with the development of a fibrous granulation tissue in the bone defect and vascularization around the plate in non-infected mice. These non-infected mice displayed elevated expression of TGF-β and PDGF genes as indicators of the bone healing processes. These non-infected mice also displayed

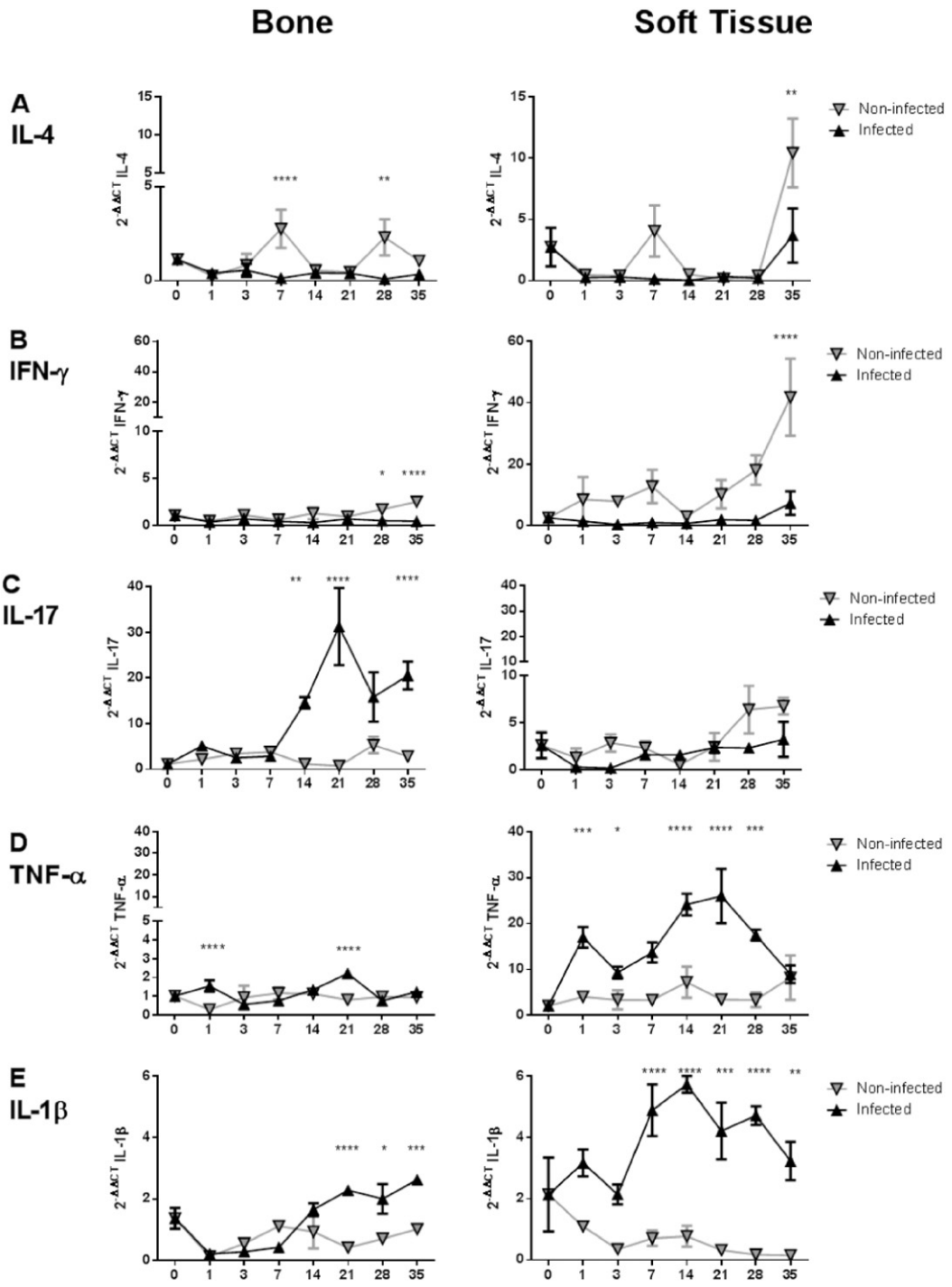

Fig. 6. Expression of selected cytokine genes in the bone and soft tissue samples in the infected and non-infected mice: bone and soft tissue samples were harvested immediately post-euthanasia and quantitative real time PCR performed on homogenized tissue. n = 6 per group, * $P < 0.05$; **$P < 0.01$; ***$P < 0.001$;****$P < 0.0001$ infected vs non-infected.

elevated expression of both IFN-γ and IL-4 genes and secretion of both cytokines at later time-points. IL-4 is an indicator of a T_H2 type immune response [27] and induces the alternative activation of macrophages (M2 macrophages) and foreign body giant cell formation. The increased expression of the IFN-γ gene and IFN-γ secretion near completion of the healing phase (day 28), indicates that a T_H1 type immune response is involved in the fracture healing process in this model. Although, IL-4 positive lymphocytes were elevated in lymph nodes from infected mice at day 28, the lack of IL-4 gene expression and IL-4 secretion from infected bone or soft tissue at the later time points suggest that these IL-4 positive cells do not migrate to the bone or soft tissue of infected animals. The role of adaptive immunity in bone healing is somewhat unclear to date [28–30], and later observation time-points may be helpful to understand this finding. Nevertheless, our data indicates that the healing response in the absence of infection appears to be characterized by a combination of a sustained T_H2 type cytokine response (indicated by IL-4) and a late T_H1 type cytokine response (indicated by IFN-γ) within the bone.

The second target of the present work was to monitor the progression of *S. aureus* infection after osteosynthesis. We used an inoculum consistent with many previous murine models of implant related bone infection [7,14,31], although this inoculum may well exceed the likely bacterial contamination of a surgical site, at least in an elective procedure or a closed fracture. A lower inoculum, reflective of the

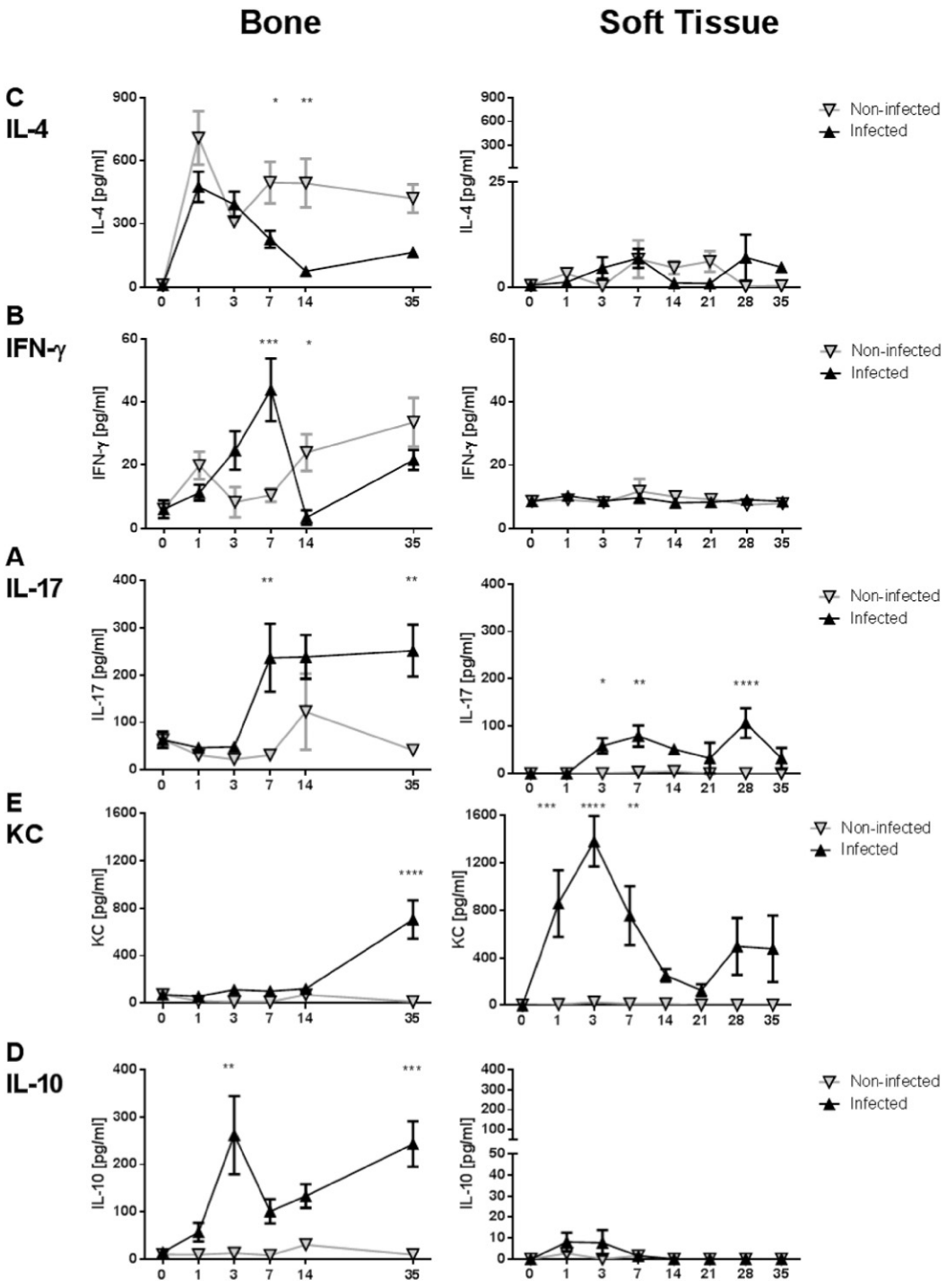

Fig. 7. Secretion of selected cytokines in supernatants of bone or soft tissue cells from infected and non-infected mice. Bone and soft tissue single cell suspensions were stimulated with PMA/ionomycin for 24 h *in vitro*: n = 6 per group, * P < 0.05; **P < 0.01; ***P < 0.001;****P < 0.0001 infected vs non-infected.

bacterial contamination levels commonly experienced in a modern surgical theater, would be interesting, though may risk spontaneous clearance of the infection. As may be expected from a virulent microorganism such as *S. aureus*, infection was persistent after surgery, leading to bone destruction and a lack of fracture healing, as observed radiographically, histologically and in the reduced expression of PDGF and TGF-β. Within 24 h of inoculation, there was a rapid increase in the number of bacteria colonizing the implant and spread of bacteria throughout the surgical site. After this initial expansion, the bacterial burden reduced and stabilized from day 7 to day 35 as the initial aggressive infection progressed to a chronic infection. The observed kinetics of bacterial numbers matches the trends reported elsewhere for intracortical pin models of implant related bone infection where an initial increase in *S. aureus* associated with a femoral trans-cortical pin was followed by a reduction and later stabilization [31]. A recently described murine osteosynthesis infection model seemed to show a similar trend, although the reported bacterial numbers were measured from wound lavage rather than from implants or tissue biopsies [21]. Histological analysis of the infected animals in this study revealed that a significant portion of the bacteria appeared to be associated in micro-colonies around bone fragments and in the necrotic soft tissue above the implant. A thin biofilm layer, approximately 5–15 μm thick, had formed

on the implant surface, although in combination with the quantitative bacteriological data, it seems this is only responsible for a portion of the bacterial burden, as significant numbers were also observed in the tissue samples. This represents an interesting observation as much of the existing orthopedic infection research focusses on the formation of biofilms on the implant surface [31,32] and less so on the surrounding tissue [33]. Of course, in the case of treating or managing such infections in human patients, the biofilm on the implant may well provide the reservoir for recurrence of infection if not removed. It would be interesting to explore antibiotic treatment with this model in future, whereby biofilm-growing bacteria may well survive and emerge as a key factor in persistence of infection. Furthermore, in a clinical situation fractures will typically involve a jagged, irregular fracture rather than a straight osteotomy. It may be that the uneven surface of the fracture would offer further dead spaces for bacterial micro-colony formation and should be a target for future studies. It should be noted however, that creation of blunt force trauma to achieve realistic fractures would also increase the burden upon the animals and likely increase the rate of exclusions due to dislocation or severe, unfixable fractures.

In terms of the immunological responses to infection, we observed evidence of a robust adaptive immune response after 1 week, as revealed by increasing numbers of cells in both local lymph nodes and spleen. In particular, IL-17 positive lymphocytes increased in the lymph node of infected animals, but not in the non-infected animals. IL-17 gene expression and *ex vivo* IL-17 secretion was also elevated in bone from infected animals, while infected soft tissue single cell suspensions increased secretion of IL-17 *ex vivo*. These observations suggest that a T_H17 response is central in *S. aureus* infection, though ultimately unsuccessful in clearing the infection in our model. T_H17 responses have been previously shown to serve a protective role in other *S. aureus* infection models, such as skin, surgical site and bloodstream infection models [34–36]. However, in our implant related bone infection model, the T_H17 response is ineffective in achieving any meaningful reduction in bacterial burden. This observation does mirror those in the cortical pin model, where IL-17 was also found to be increased, though once again unable to eradicate the *S. aureus* infection [31]. In fact, elevated IL-17 may be somewhat counterproductive in an implant-bone infection, as IL-17 has also been shown to induce osteoclastogenesis [37,38].

Interestingly, the immune response in the soft tissue differed from the bone in a number of ways. For example, IL-17 increases were more apparent in infected bone, whilst increases in KC secretion, TNF-α and IL-1β gene expression were greater in infected soft tissues. The pro-inflammatory cytokines KC, TNF-α and IL-1β are typically expressed at much higher levels by innate immune cells such as macrophages or dendritic cells, compared to lymphocytes, suggesting a more pronounced innate immune response in infected soft tissue compared to infected bone. The quantitative bacteriological evaluation suggests that bacterial burden is equivalent in the different tissues over time, indicating that both the IL-17-led bone response and the pro-inflammatory cytokine-led soft tissue response are both ineffectual in clearing implant related bone and soft tissue infections. The well-described recalcitrance of biofilm to host defenses may be critical in this regard as the biofilm occupies the interface between the soft and hard tissues. Recently, persistence of infection in a murine prosthetic joint infection model has been at least partially attributed to myeloid derived suppressor cell recruitment through IL-12 [39]. Unfortunately, our mRNA data did not detect IL-12 and thus further experiments are required to determine if such mechanisms could contribute to *S. aureus* persistence in our model.

In conclusion, we have described a murine model of infection after osteosynthesis. Within 4 weeks of surgery, the fracture heals and most responses return to or approach baseline in non-infected animals. The characteristics of the non-infected mice were seen to be a lack of changes in the lymph node and spleen total cell numbers; brief elevations in IFN-γ and IL-4 positive lymphocytes in the lymph node in the first post-operative day; and increased IFN-γ and IL-4 gene expression and cytokine secretion at various times throughout the healing phase. In the presence of a bacterial contamination, the response is dramatically different: increased proportions of IL-17 and IL-10 positive lymphocytes; increased IL-17, TNF-α and IL-1β gene expression; and increased IL-17, IL-10 and KC secretion in local bone and/or soft tissue cells.

The model provides a closer evaluation of the immune response as it pertains to a post-traumatic fracture. This study revealed consistencies with foreign-body bone infection models, however, the presence of an osteotomy and biomechanically influenced fracture healing enabled evaluation of the specific processes involved in infection after osteosynthesis. Crucially, we could show that the persistence of the infection is linked with an altered immune profile secondary to early non-specific responses driven by the presence of the fracture and the implant.

Supplementary data to this article can be found online at http://dx.doi.org/10.1016/j.bone.2015.10.014.

Acknowledgements

This work was funded by AOTrauma as part of the Clinical Priority Program on Bone Infection (Grant number AR2011_8). Pamela Furlong, Iris Keller, Sandra Thoeny, Nora Goudsouzian and Barbara Stanic of the AO Research Institute Davos are thanked for technical assistance and manuscript review.

References

[1] R.O. Darouiche, Treatment of infections associated with surgical implants, N. Engl. J. Med. 350 (2004) 1422–1429.
[2] M.J. Patzakis, J. Wilkins, Factors influencing infection rate in open fracture wounds, Clin. Orthop. Relat. Res. (1989) 36–40.
[3] S.D. Elek, P.E. Conen, The virulence of *Staphylococcus pyogenes* for man; a study of the problems of wound infection, Br. J. Exp. Pathol. 38 (1957) 573–586.
[4] R.M. Donlan, J.W. Costerton, Biofilms: survival mechanisms of clinically relevant microorganisms, Clin. Microbiol. Rev. 15 (2002) 167–193.
[5] L.R. Thurlow, M.L. Hanke, T. Fritz, A. Angle, A. Aldrich, S.H. Williams, I.L. Engebretsen, K.W. Bayles, A.R. Horswill, T. Kielian, *Staphylococcus aureus* biofilms prevent macrophage phagocytosis and attenuate inflammation in vivo, J. Immunol. 186 (2011) 6585–6596.
[6] C.E. Heim, D. Vidlak, T.D. Scherr, J.A. Kozel, M. Holzapfel, D.E. Muirhead, T. Kielian, Myeloid-derived suppressor cells contribute to *Staphylococcus aureus* orthopedic biofilm infection, J. Immunol. 192 (2014) 3778–3792.
[7] R. Prabhakara, J.M. Harro, J.G. Leid, A.D. Keegan, M.L. Prior, M.E. Shirtliff, Suppression of the inflammatory immune response prevents the development of chronic biofilm infection due to methicillin-resistant *Staphylococcus aureus*, Infect. Immun. 79 (2011) 5010–5018.
[8] W.G. DeLong Jr., C.T. Born, Cytokines in patients with polytrauma, Clin. Orthop. Relat. Res. (2004) 57–65.
[9] P.V. Giannoudis, Current concepts of the inflammatory response after major trauma: an update, Injury 34 (2003) 397–404.
[10] P. Lichte, P. Kobbe, D. Dombroski, H.C. Pape, Damage control orthopedics: current evidence, Curr Opin Crit. Care 18 (2012) 647–650.
[11] H.C. Pape, R. Marcucio, C. Humphrey, C. Colnot, M. Knobe, E.J. Harvey, Trauma-induced inflammation and fracture healing, J. Orthop. Trauma 24 (2010) 522–525.
[12] P. Kolar, T. Gaber, C. Perka, G.N. Duda, F. Buttgereit, Human early fracture hematoma is characterized by inflammation and hypoxia, Clin. Orthop. Relat. Res. 469 (2011) 3118–3126.
[13] K. Schmidt-Bleek, H. Schell, J. Lienau, N. Schulz, P. Hoff, M. Pfaff, G. Schmidt, C. Martin, C. Perka, F. Buttgereit, H.D. Volk, G. Duda, Initial Immune Reaction and Angiogenesis in Bone Healing, 2012.
[14] D. Li, K. Gromov, K. Soballe, J.E. Puzas, R.J. O'Keefe, H. Awad, H. Drissi, E.M. Schwarz, Quantitative mouse model of implant-associated osteomyelitis and the kinetics of microbial growth, osteolysis, and humoral immunity, J. Orthop. Res. 26 (2008) 96–105.
[15] S.A. Horst, V. Hoerr, A. Beineke, C. Kreis, L. Tuchscherr, J. Kalinka, S. Lehne, I. Schleicher, G. Kohler, T. Fuchs, M.J. Raschke, M. Rohde, G. Peters, C. Faber, B. Loffler, E. Medina, A novel mouse model of *Staphylococcus aureus* chronic osteomyelitis that closely mimics the human infection: an integrated view of disease pathogenesis, Am J Pathol. 181 (2012) 1206–1214.
[16] Y.H. An, R.J. Friedman, Animal models of orthopedic implant infection, J. Invest. Surg. 11 (1998) 139–146.
[17] L. Calabro, C. Lutton, A. Din, R.G. Richards, T.F. Moriarty, Animal models of orthopedic implant-related infection, in: T.F. Moriarty, S.A.J. Zaat, H.J. Busscher (Eds.), Biomaterials Associated Infection, Springer, New York 2013, pp. 273–304.

[18] T. Hamza, M. Dietz, D. Pham, N. Clovis, S. Danley, B. Li, Intra-cellular *Staphylococcus aureus* alone causes infection in vivo, Eur. Cell Mater. 25 (2013) 341–350 (discussion 350).
[19] B. Li, B. Jiang, B.M. Boyce, B.A. Lindsey, Multilayer polypeptide nanoscale coatings incorporating IL-12 for the prevention of biomedical device-associated infections, Biomaterials 30 (2009) 2552–2558.
[20] T. Histing, P. Garcia, R. Matthys, M. Leidinger, J.H. Holstein, A. Kristen, T. Pohlemann, M.D. Menger, An internal locking plate to study intramembranous bone healing in a mouse femur fracture model, J. Orthop. Res. 28 (2010) 397–402.
[21] C.D. Windolf, W. Meng, T.T. Logters, C.R. MacKenzie, J. Windolf, S. Flohe, Implant-associated localized osteitis in murine femur fracture by biofilm forming *Staphylococcus aureus*: a novel experimental model, J. Orthop. Res. 31 (2013) 2013–2020.
[22] D. Campoccia, L. Montanaro, T.F. Moriarty, R.G. Richards, S. Ravaioli, C.R. Arciola, The selection of appropriate bacterial strains in preclinical evaluation of infection-resistant biomaterials, Int. J. Artif. Organs 31 (2008) 841–847.
[23] T.F. Moriarty, L. Debefve, L. Boure, D. Campoccia, U. Schlegel, R.G. Richards, Influence of material and microtopography on the development of local infection in vivo: experimental investigation in rabbits, Int. J. Artif. Organs 32 (2009) 663–670.
[24] E.T. Rochford, A.H. Poulsson, V.J. Salavarrieta, P. Lezuo, R.G. Richards, T.F. Moriarty, Bacterial adhesion to orthopaedic implant materials and a novel oxygen plasma modified PEEK surface, Colloids Surf. B: Biointerfaces **113C** (2013) 213–222.
[25] I. Gröngröft, P. Heil, R. Matthys-Mark, P. Lezuo, A. Tami, S. Perren, P. Montavon, K. Ito, Fixation compliance in a mouse fracture model induces two different processes of fracture healing but does not lead to delayed union, J. Biomech. 42 (2009) 2089–2096.
[26] R. Steck, M. Ueno, L. Gregory, N. Rijken, M.E. Wullschleger, M. Itoman, M.A. Schuetz, Influence of internal fixator flexibility on murine fracture healing as characterized by mechanical testing and microCT imaging, J. Orthop. Res. 29 (2011) 1245–1250.
[27] M. Akdis, S. Burgler, R. Crameri, T. Eiwegger, H. Fujita, E. Gomez, S. Klunker, N. Meyer, L. O'Mahony, O. Palomares, C. Rhyner, N. Ouaked, A. Schaffartzik, W. Van De Veen, S. Zeller, M. Zimmermann, C.A. Akdis, Interleukins, from 1 to 37, and interferon-gamma: receptors, functions, and roles in diseases, J. Allergy Clin. Immunol. 127 (701–721) (2011) e701–e770.
[28] N.T. Colburn, K.J. Zaal, F. Wang, R.S. Tuan, A role for gamma/delta T cells in a mouse model of fracture healing, Arthritis Rheum. 60 (2009) 1694–1703.
[29] I. Konnecke, A. Serra, T. El Khassawna, C. Schlundt, H. Schell, A. Hauser, A. Ellinghaus, H.D. Volk, A. Radbruch, G.N. Duda, K. Schmidt-Bleek, T and B cells participate in bone repair by infiltrating the fracture callus in a two-wave fashion, Bone 64 (2014) 155–165.
[30] D. Toben, I. Schroeder, T. El Khassawna, M. Mehta, J.E. Hoffmann, J.T. Frisch, H. Schell, J. Lienau, A. Serra, A. Radbruch, G.N. Duda, Fracture healing is accelerated in the absence of the adaptive immune system, J. Bone Miner. Res. Off. J. Am. Soc. Bone Miner. Res. 26 (2011) 113–124.
[31] R. Prabhakara, J.M. Harro, J.G. Leid, M. Harris, M.E. Shirtliff, Murine immune response to a chronic *Staphylococcus aureus* biofilm infection, Infect. Immun. 79 (2011) 1789–1796.
[32] R.A. Brady, J.G. Leid, A.K. Camper, J.W. Costerton, M.E. Shirtliff, Identification of *Staphylococcus aureus* proteins recognized by the antibody-mediated immune response to a biofilm infection, Infect. Immun. 74 (2006) 3415–3426.
[33] S. Zaat, C. Broekhuizen, M. Riool, Host tissue as a niche for biomaterial-associated infection, Future Microbiol 5 (2010) 1149–1151.
[34] J.S. Cho, E.M. Pietras, N.C. Garcia, R.I. Ramos, D.M. Farzam, H.R. Monroe, J.E. Magorien, A. Blauvelt, J.K. Kolls, A.L. Cheung, G. Cheng, R.L. Modlin, L.S. Miller, IL-17 is essential for host defense against cutaneous *Staphylococcus aureus* infection in mice, J. Clin. Invest. 120 (2010) 1762–1773.
[35] L. Lin, A.S. Ibrahim, X. Xu, J.M. Farber, V. Avanesian, B. Baquir, Y. Fu, S.W. French, J.E. Edwards Jr., B. Spellberg, Th1-Th17 cells mediate protective adaptive immunity against *Staphylococcus aureus* and *Candida albicans* infection in mice, PLoS Pathog. 5 (2009), e1000703.
[36] B.M. Maher, M.E. Mulcahy, A.G. Murphy, M. Wilk, K.M. O'Keeffe, J.A. Geoghegan, E.C. Lavelle, R.M. McLoughlin, Nlrp-3-driven interleukin 17 production by gammadeltaT cells controls infection outcomes during *Staphylococcus aureus* surgical site infection, Infect. Immun. 81 (2013) 4478–4489.
[37] S.J. Moon, I.E. Ahn, H. Jung, H. Yi, J. Kim, Y. Kim, S.K. Kwok, K.S. Park, J.K. Min, S.H. Park, H.Y. Kim, J.H. Ju, Temporal differential effects of proinflammatory cytokines on osteoclastogenesis, Int. J. Mol. Med. 31 (2013) 769–777.
[38] S. Kotake, N. Udagawa, N. Takahashi, K. Matsuzaki, K. Itoh, S. Ishiyama, S. Saito, K. Inoue, N. Kamatani, M.T. Gillespie, T.J. Martin, T. Suda, IL-17 in synovial fluids from patients with rheumatoid arthritis is a potent stimulator of osteoclastogenesis, J. Clin. Invest. 103 (1999) 1345–1352.
[39] C.E. Heim, D. Vidlak, T.D. Scherr, C.W. Hartman, K.L. Garvin, T. Kielian, IL-12 promotes myeloid-derived suppressor cell recruitment and bacterial persistence during *Staphylococcus aureus* orthopedic implant infection, J. Immunol. 194 (2015) 3861–3872.